PERGAMON

Neural Networks 14 (2001) 845–863

Neural Networks

www.elsevier.com/locate/neunet

2001 Special issue

A pulsed neural network model of bursting in the basal ganglia

Mark D. Humphries*, Kevin N. Gurney

Department of Psychology, University of Sheffield, Sheffield, S10 2TP, UK

Received 11 October 2000; revised 26 March 2001; accepted 26 March 2001

Abstract

We present new techniques for extending the functionality of spiking neurons which allow the incorporation of several aspects of neuron function previously confined to the domain of low level ion-channel based models. These aspects include spontaneous (or endogenous) firing, the complex interaction of multiple ion-species and the spatial distribution of synaptic contacts over the cell membrane. These ideas are applied to a neural circuit consisting of the cortex and a subset of the nuclei in the basal ganglia—the subthalamic nucleus (STN) and the external segment of the globus pallidus (GPe). This circuit has been studied extensively in vitro by Plenz and Kitai [Plenz, D., & Kitai, S. T. (1999). A basal ganglia pacemaker formed by the subthalamic nucleus and external globus pallidus. *Nature*, *400* 677–682] whose data we use to constrain our model. With respect to this circuit, we have obtained three main results. First, that its characteristic burst firing is due to a Ca^{2+} current mediated mechanism. Second, that noise can assist in the generation of bursting and, paradoxically, stabilise the network behaviour under synaptic weight variations. Third, that a variety of dendritic processing is necessary in order to obtain the full range of bursting behaviour. © 2001 Published by Elsevier Science Ltd.

Keywords: Spiking neuron; STN; GPe; Basal ganglia; Ca^{2+} currents; Noise; Compartmental model

1. Introduction

Neuron models range in complexity from simple Boolean-valued McCulloch and Pitts type units (Gurney, 1997) to those that attempt to model the dynamics of ionic currents (channels) in the neuron membrane and that incorporate geometric affects in multiple membrane compartments (Segev, Fleshman & Burke, 1989). Between these two extremes lies a spectrum of possible model neuron types. The level of computing power necessary to simulate a network of multi-compartmental units for a significant period of simulated real time is prohibitive, and likely to remain so in the near future. More pertinently, the dimensionality of the parameter space becomes too large to explore effectively in even a simple network. While the parameters may be bounded by neurophysiological data, there always remains some uncertainty in their values and, moreover, the contribution that each parameterised mechanism makes to neural circuit behaviour becomes increasingly difficult to evaluate.

With this in mind, Maass (1997) has distinguished three generations of model neuron that are effectively usable in networks: perceptrons, activation function units (e.g. those using sigmoidal output functions) and spiking units. Spiking model units (Gerstner, 1999; Maass, 1997) attempt to mimic *phenomenologically* the dynamics of the membrane potential u by combining a series of function kernels that mimic different mechanistic components of u. The development of spiking neuron models invites an intriguing question: is it possible, using this family of models, to simulate some of the complex dynamics shown by real neurons (and which is certainly within the grasp of the potentially more powerful models based explicitly on membrane compartments)?

The main objective of this paper is to show that, at least for some neural circuits, this question has an affirmative answer. We achieve this by exhibiting a model of a neural circuit that has been studied in isolation and which displays a rich signal behaviour (Plenz & Kitai, 1999). The circuit in question is part of the basal ganglia (BG), a group of subcortical brain structures that are implicated in motor control and behavioural regulation (Hikosaka, 1991; Redgrave, Prescott & Gurney, 1999). The circuit consists of the reciprocal loop containing two BG sub-nuclei—the subthalamic nucleus (STN) and external segment of the globus pallidus (GPe). The gross anatomical connectivity of these and associated structures (the striatum and cortex) is shown in Fig. 1. STN is a source of excitation within BG (Gerfen & Wilson, 1996) and projects to GPe. GPe sends GABAergic (inhibitory) projections to STN and the striatum (a major

* Corresponding author. Tel.: +44-114-2226523.
E-mail address: m.d.humphries@shef.ac.uk (M.D. Humphries).

0893-6080/01/$ - see front matter © 2001 Published by Elsevier Science Ltd.
PII: S0893-6080(01)00060-0

Nomenclature

c^{+}_{ss}	Weight of the STN internal axon collaterals
c^{+}_{sg}	Weight of the STN → GPe connections
c^{-}_{gs}	Weight of the GPe → STN connections
c^{+}_{cs}	Weight of the cortex → STN connections
J^{*}_{prox}	Maximum post-synaptic current due to proximal GPe synapses
J^{*}_{soma}	Maximum post-synaptic current due to somatic GPe synapses
C	Membrane capacitance
τ_m	Membrane time constant
τ_s	Synaptic time constant
θ	Firing threshold
α_{Ca}	Level of current input due to the Ca^{2+} mechanism
θ_{Ca}	The Ca^{2+} mechanism triggering threshold
t_1	Period of pulse component of Ca^{2+} current
t_2	Period of ramp component of Ca^{2+} current
I_{spon}	The current causing spontaneous firing
I_{noise}	The current input due to noise
I_{ref}	The current due to the relative refractory period
I_{syn}	The current due to the pre-synaptic spikes
I_{Ca}	The current due to the Ca^{2+} mechanism

input nucleus in the BG) sends GABAergic projections to GPe. Both the striatum and STN receive glutamatergic (excitatory) cortical input (Bevan, Francis & Bolam, 1995; Turner & DeLong, 2000). Finally, STN contains excitatory connections internal to this nucleus (Fujimoto & Kita, 1993).

As well as offering a rich and well described neural signal repertoire, the STN–GPe loop is of particular interest to us as part of our wider computational study of the basal ganglia (Gurney, Prescott & Redgrave, 2001a,b; Humphries & Gurney, 1999; Redgrave et al., 1999). This has implications for the approach we take in modelling the network architecture that is detailed in Section 2.

The work of Plenz and Kitai (1999) was based on single- and multi-unit recordings from an organotypic culture in vitro obtained from neonatal rats. The mature culture contained STN, GPe, striatum, and cortex as shown in Fig. 1. The STN–GPe circuit showed synchronised spontaneous burst firing between STN neuron pairs and STN–GPe neuron pairs at two main burst frequencies—0.4 and 0.8 Hz—in the complete culture (cortex-intact condition). Furthermore, lesioning the cortex caused the bursting to occur predominantly at 0.8 Hz (cortex-disconnected condition). Striatal lesions had no affect on bursting frequency. This is not surprising as striatal neurons are generally silent unless driven by co-ordinated afferent input which shifts them from their DOWN-state to their firing-ready UP-state (Gerfen & Wilson, 1996; Wickens & Wilson, 1998). Therefore, the GPe receives little or no inhibitory input from striatum and, hence, the striatum has no affect on the bursting in the STN–GPe loop. Plenz and Kitai concluded that the STN–GPe circuit could act as a central pacemaker for the basal ganglia, controlling temporal aspects of processing. This suggests the hypothesis that the bursting is due to intrinsic properties of the STN–GPe circuit which can be modulated by cortical input. In particular, we make the hypothesis that the bursting behaviour observed by Plenz and Kitai was initiated by the Ca^{2+} current-based mechanism described by Beurrier, Congar, Bioulac and Hammond (1999). Under this assumption, our model was able to explain the mono-modal bursting without cortical input, but was unable to replicate the diversity of behaviour that occurred with cortical input. However, we then went on to incorporate the affects on the membrane potential due to the relative distribution of GPe synapses over the surface of neurons in STN. This extra degree of realism gave the model the ability to show behaviour similar to that observed by Plenz and Kitai in their cultures with cortex intact.

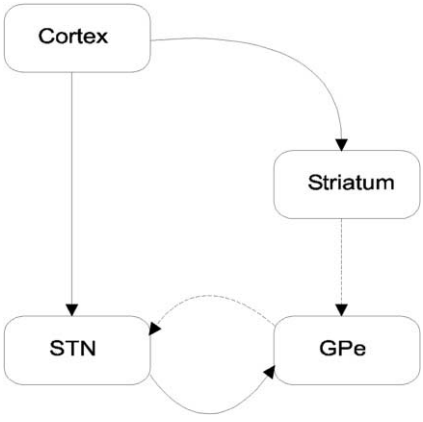

Fig. 1. The basal ganglia circuit cultured by Plenz and Kitai (1999). Solid line: excitatory; dashed line: inhibitory.

Details of the Ca^{2+} current and synaptic distributions, together with their respective model counterparts are given in Section 2. However, the underlying methodology that allows their incorporation in our model is to continue in the spirit adopted in developing the basic spiking neuron model itself. That is, we suppose that each further contribution to the membrane potential may be modelled using an additional functional component, explicitly crafted to capture the phenomenological time course of the corresponding potential component. We are not concerned, at this level of modelling, in deriving the functional form of the membrane potential from more fundamental physical processes (such as ion channels). This phenomenological approach is, we believe, the key to extending the spiking neuron models to a wide range of neural classes and circuits. This paper describes an application of this novel technique that incorporates a range of additional contributions to the membrane potential in STN neurons.

2. Method

2.1. The model neuron

The model neuron is based on the integrate-and-fire neuron described by Gerstner (1999) (see also Brunel & Sergi, 1998). We first describe a basic version of this neuron before going on to incorporate additional features in Section 2.2.

The total membrane current $I(t)$ is given by the sum of capacitive and resistive components

$$I(t) = \frac{u(t)}{R} + C\frac{\mathrm{d}u}{\mathrm{d}t} \tag{1}$$

where C is the membrane capacitance, R its resistance, and u the membrane potential. The product $\tau_\mathrm{m} = RC$ has dimensions of time and determines a characteristic time scale (the *membrane time constant*) for signals to change in the membrane. Using the definition of τ_m in Eq. (1) gives

$$\tau_\mathrm{m}\frac{\mathrm{d}u}{\mathrm{d}t} = -u(t) + RI(t) \tag{2}$$

Note that, with no input current, the equilibrium value of u is zero.

The model neuron 'fires' if u reaches a threshold θ from below; that is, $u = \theta$ and $\mathrm{d}u/\mathrm{d}\theta \equiv u' > 0$. We denote the set of firing times of the neuron by F where $F = \{t^{(1)}, t^{(2)}, \ldots, t^{(n)}\}$. After firing, the membrane potential is reset to a value u_r, a process which models the neuron's relative refractory period after firing. In spite of this reset, it is possible that the membrane is being driven (by synaptic input or injection current) so hard that it very rapidly reaches θ again. However, a neuron also has a fixed time, the absolute refractory period τ_abs, during which it may not fire a spike regardless of the strength of input. This is modelled by stopping the solution of Eq. (2) for τ_abs and forcing the membrane potential to zero for this time. The absolute refractory period will limit the theoretical maximum firing rate of an individual model neuron to $1/\tau_\mathrm{abs}$ Hz. The value of τ_abs is set to a conservative value so that the total refractory period (the combination of the absolute and relative refractory periods) is biologically plausible.

The current $I(t)$ is constituted from three sources. First, $I(t)$ contains a contribution $I_\mathrm{syn}(t)$ from synaptic input. Let Γ be the set of afferents to the neuron under consideration (we drop any index for this neuron to simplify notation). Let c_j represent the strength of connection (the 'weight') from afferent j and suppose that each current pulse is shaped according to some kernel function $\alpha(s)$. Then, assuming that post-synaptic potentials (PSPs) combine additively

$$I_\mathrm{syn}(t) = \sum_{j\in\Gamma} c_j \sum_{t_j^{(f)}\in F^j} \alpha(t - t_j^{(f)}) \tag{3}$$

Usually, we take $\alpha(s)$ to be a step followed by exponential decay

$$\alpha(s) = \frac{1}{\tau_\mathrm{s}} \mathrm{e}^{-s/\tau_\mathrm{s}} H(s) \tag{4}$$

where $H(s)$ is the Heaviside step function which is zero for $s \leq 0$ and is one otherwise, and τ_s is the synaptic time constant. Hence, the second term of Eq. (3) models the temporal decay of the current charge caused by the arrival of a pre-synaptic spike.

Second, it is possible to model the post-firing reset condition (and thereby the relative refractory period) using a current I_ref that consists of a series of Dirac δ pulses.

$$I_\mathrm{ref} = -C(\theta - u_\mathrm{r}) \sum_{t_i^{(f)}\in F_i} \delta(t - t_i^{(f)}) \tag{5}$$

Finally, there is a noise component, I_noise which models the many stochastic processes occurring in the cell membrane (Gerstner, 1999). This current ensures that membrane potentials of different units with identical inputs and parameters are not the same. Hence, Eq. (2) becomes

$$\tau_\mathrm{m}\frac{\mathrm{d}u}{\mathrm{d}t} = -u(t) + R[I_\mathrm{syn}(t) + I_\mathrm{ref}(t) + I_\mathrm{noise}(t)] \tag{6}$$

2.2. Extending the model

In this section, we describe how further contributions to the membrane potential may be added to the basic spiking neural model outlined above. In all that follows, it is assumed that we are dealing with an STN neuron; GPe neurons are described by equations of the form (6).

2.2.1. STN spontaneous output

At rest, in vivo, an STN neuron has a tonic firing rate of 10–30 Hz (Fujimoto & Kita, 1993; Wichmann, Bergman & DeLong, 1994) due to a combination of cortical input and a rhythmic, spontaneous oscillation at 3–4 Hz that can be

observed in vitro (Bevan & Wilson, 1999). That this residual spontaneous firing rate is not due to excitatory input is indicated by its presence after the application of glutamate receptor blockers (Bevan & Wilson, 1999). It must, therefore, be a property intrinsic to the STN neuron membrane and has been ascribed to a Na^+ current (Beurrier, Bioulac & Hammond, 2000).

To model this spontaneous output we added a small constant current I_{spon} to the membrane potential equation (6):

$$\tau_m \frac{du}{dt} = -u(t) + R[I_{syn}(t) + I_{spon}(t) + I_{ref}(t) + I_{noise}(t)] \quad (7)$$

The effect of this current is to make STN units output a very low frequency spike train which is necessarily irregular due to the noise component in Eq. (7).

2.2.2. Modelling the Ca^{2+} mechanism

This section is based on the work of Beurrier et al. (1999) that explored bursting in STN neurons. The central finding of this study was that STN neurons could be made to burst-fire in vitro by the application of a small hyperpolarising current. The sudden increase in activity after a hyperpolarisation leads to the term 'rebound' burst firing for this phenomenon. Beurrier et al. (1999) attributed this counter-intuitive result to the following sequence of ion channel activity. The hyperpolarisation activates a Ca^{2+} current $I_{T/R}$, which depolarises the membrane until it crosses the activation threshold (from below) for the Ca^{2+} current I_L. Immediately after this, $I_{T/R}$ deactivates. The I_L current is self sustaining since it increases with the depolarisation of the membrane potential. The membrane potential then reaches a plateau phase where action potentials are continuously generated because the membrane potential is continuously above firing threshold. However, the high levels of intra-cellular Ca^{2+} now initiate a Ca^{2+} activated K^+ current I_K which acts to hyperpolarise the membrane. I_K is slightly larger than I_L, resulting in a decrease in membrane potential and the diminution of the burst. Repolarisation occurs when the I_L deactivation threshold is passed (from above) and I_L rapidly deactivates. The cycle is then ready to begin again.

Our model of this cycle of current activation and deactivation is based on a simple piecewise linear approximation $I_{Ca}(t)$ of the net current across the membrane. No attempt is made to model the detailed dynamics of each component current ($I_{T/R}$, I_L, I_K) or their complex interaction. Thus, we suppose that I_{Ca} is activated by the membrane potential hyperpolarising below a threshold θ_{Ca}. There is then an initial step pulse in I_{Ca} of duration t_1 and height α_{Ca} which models the rapid depolarisation to the start of the plateau phase caused by the Ca^{2+} T/R- and L-type currents. This is then followed by a slowly declining ramp (of duration t_2) which models the slow decrease of net current into the membrane via the combined action of I_L and I_K. Our pseudo-current I_{Ca} may be expressed formally by

$$I_{Ca} = \begin{cases} 0 & \text{if } u > \theta_{Ca} \\ \alpha_{Ca} & \text{if } u < \theta_{Ca} \text{ and } 0 < t < t_1 \\ -\alpha_{Ca}(t - t_1)/t_2 + \alpha_{Ca} & \text{if } u < \theta_{Ca} \text{ and } t_i < t < t_2 \end{cases} \quad (8)$$

where t is time since the beginning of period t_1. Periods t_1 and t_2 have values commensurate with the fact that STN bursts can last several hundred milliseconds (Magill, Bolam & Bevan, 2000; Plenz & Kitai, 1999). The level of α_{Ca} determines the intra-burst firing frequency: the larger α_{Ca}, the faster the neuron will fire during the burst. An initial value of 7.5 μA for α_{Ca} was determined empirically by simulation of a single STN unit. A simulated hyperpolarising current was injected into the unit and the value of α_{Ca} was altered until the unit fired at between 80 and 100 Hz during the initial period of the burst. These target firing frequencies were determined from Plenz and Kitai's data for STN neurons bursting at 0.8 Hz because these units were not receiving any input from cortex. The resulting STN firing pattern is shown in Fig. 2.

With the inclusion of I_{Ca} the membrane equation for STN (7) is now modified to (dropping (t) for clarity)

$$\tau_m \frac{du}{dt} = -u(t) + R[I_{syn}(t) + I_{spon} + I_{ref} + I_{Ca} + I_{noise}] \quad (9)$$

2.2.3. A quasi-compartmental model

The patterns of synaptic contact on an STN neuron from each of its afferent species are not identical. Cortical and STN axon collaterals synapse predominantly on the distal dendrites (Gerfen & Wilson, 1996). GPe, on the other hand, synapses on distal dendrites, proximal dendrites, and the soma in roughly equal proportions (with a slight preference for proximal dendrites) (Bevan, Clarke & Bolam, 1997; Gerfen & Wilson, 1996).

Synapses on distal dendrites are associated with the production of PSPs that tend to combine additively (Borst & Egelhaaf, 1994). This is just the kind of PSP interaction modelled by Eq. (3). However, inhibitory synapses on proximal dendrites and the soma often tend to have a multiplicative or 'gating' affect on distal synaptic input (Blomfield, 1974), often referred to as 'shunting inhibition'. This means that they can substantially attenuate any PSPs initiated on distal dendrites or even 'veto' their affect completely (Shepherd & Brayton, 1987). Hence, given the synaptic contact patterns described above, and the provision of inhibitory afferents to STN by GPe, it seems possible that around 70% of GPe synapses in a given STN neuron may exert a shunting inhibition affect on the cortical, STN axon collateral and (remaining) GPe input.

One method of modelling the different synaptic contact patterns would be to create a full three compartment model neuron (Segev et al., 1989) with compartments for distal and proximal dendrites, and the soma (see Fig. 3). This would

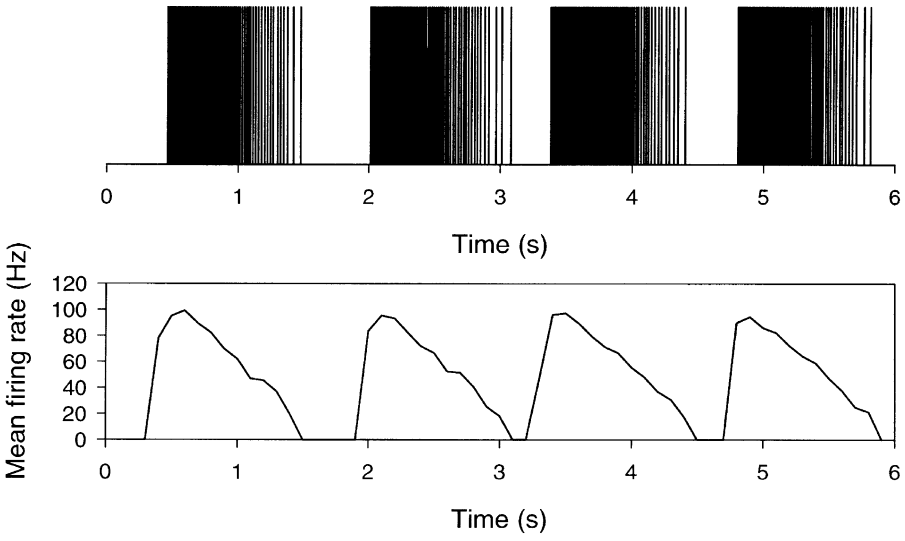

Fig. 2. Top: spike train of an isolated simulated STN unit with the Ca^{2+} mechanism. The bursts show the stereotypical initial rapid firing period followed by a decay in rate as the Ca^{2+} current deactivates. Bottom: binned inter-spike interval data for the unit, showing maximum firing rates between 80 and 100 Hz. Simulation parameters were: $t_1 = 200$; $t_2 = 1000$; $\alpha_{Ca} = 7.5$.

require modelling the temporal evolution of signals as they are transmitted across compartments, together with any inter-compartment attenuation. However, in keeping with our aim to retain the simplicity of the model neuron, the addition of synaptic input patterning is accomplished by assuming that these inter-compartmental features are of second order compared with the main arithmetical processing due to inhibitory signal gating near, and within, the cell soma. We, therefore, model the main arithmetic signal combinations in a single 'compartment' while respecting the spatially separated contributions to this processing described in Fig. 3.

Let Γ_p be the set of GPe afferents to an STN neuron that make contact with that neuron's proximal dendritic compartment and let J_{prox} be the total additive synaptic

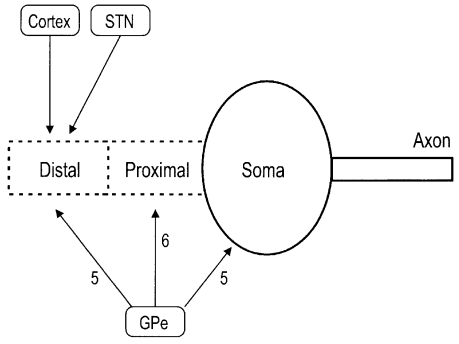

Fig. 3. Schematic representation of an STN quasi-compartmental model neuron. Cortical and intra-nucleus STN axon collateral projections synapse predominantly on the distal dendrites. GPe projections synapse on the distal and proximal dendrites and on the soma which make 31, 39 and 30%, respectively, of the GPe synapses on a single STN neuron (Gerfen & Wilson, 1996). These values correspond to a 5:6:5 ratio of GPe inputs to a single STN unit in the network.

current input from GPe on that compartment so that, from Eq. (3)

$$J_{prox}(t) = \sum_{j \in \Gamma_p} c_{gs}^{-} \sum_{t_j^{(f)} \in F^j} \alpha(t - t_j^{(f)}) \tag{10}$$

where c_{gs}^{-} is a measure of the synaptic strength between GPe and STN. The maximum value any individual component of the sum in Eq. (10) can take is c_{gs}^{-}/τ_s, since $\alpha(s)$ is given by Eq. (4). If $J_{prox}^{*} = |\Gamma_p| c_{gs}^{-}/\tau_s$, then $J_{prox}(t) \leq J_{prox}^{*}$. Now put

$$h_{prox}(t) = 1 - \frac{J_{prox}(t)}{J_{prox}^{*}} \tag{11}$$

where $0 \leq h_{prox}(t) \leq 1$. $h_{prox}(t)$, when combined multiplicatively with other synaptic input, represents an inhibitory gating factor that attenuates that input.

A similar process may be used to model somatic inhibitory gating. Thus, if Γ_s is the number of somatic afferents from GPe, define

$$J_{soma}(t) = \sum_{j \in \Gamma_s} c_{gs}^{-} \sum_{t_j^{(f)} \in F^j} \alpha(t - t_j^{(f)}) \tag{12}$$

and if $J_{prox}^{*} = |\Gamma_p| c_{gs}^{-}/\tau_s$ then put

$$h_{soma}(t) = 1 - \frac{J_{soma}(t)}{J_{soma}^{*}} \tag{13}$$

Let I_{dist} be the current due to distal dendritic input where I_{dist} is of the form in Eq. (3) with contributions from GPe and STN. We assume that GPe gating on proximal dendrites attenuates I_{dist} so that the contribution from distal afferents becomes $h_{prox}(t) I_{dist}$. Further, we suppose that the somatic gating can affect, not only the proximal dendrites, but also I_{spon} which represents an intrinsic Na^{+} current which is presumably effective at the soma. Thus, the membrane

Table 1
Model neuron output firing rate (in Hertz) in response to varying the number of inputs and the mean input firing rate

Mean input frequency (Hz)	Number of inputs (weight)						
	2 (96)	8 (24)	16 (12)	32 (6)	64 (3)	128 (1.5)	192 (1)
2	1	0	0	0	0	0	0
8	5	3	2	2	2	2	2
16	16	15	14	14	14	14	14
32	32	32	34	34	35	35	35
64	63	64	67	68	68	69	69
128	86	116	123	123	124	124	124

equation for STN neurons now becomes (dropping (t) for clarity)

$$\tau_{\mathrm{m}} \frac{\mathrm{d}u}{\mathrm{d}t} = -u + R[(I_{\mathrm{dist}} h_{\mathrm{prox}} + I_{\mathrm{spon}}) + I_{\mathrm{ref}} + I_{\mathrm{Ca}} + I_{\mathrm{noise}}] \tag{14}$$

2.3. Network design

As noted in the Introduction, this case-study of the STN–GPe reciprocal loop is also part of a wider programme of work on modelling the basal ganglia (Gurney et al., 2001b; Gurney, Redgrave & Prescott, 1998; Humphries & Gurney, 1999). In developing these models, we have determined two features of the general architecture of Fig. 1 that we carry over to the network design described here. First, BG is topographically arranged into functionally separated *channels* (Gerfen & Wilson, 1996; Hoover & Strick, 1993, 1999; Joel & Weiner, 1997). Furthermore, we adopt a simplified version of this arrangement in which the channels are represented by discrete groups of neurons. In general, therefore, we have assumed that, throughout basal ganglia, there is no inter-channel cross-talk. The crucial exception to this concerns projections from STN; evidence from studies by Hazrati & Parent (1992a,b) show that STN supplies diffuse projections to its target nuclei. In the current paper this anatomical feature is modelled using full connectivity in which every STN unit projects to every GPe unit. The discrete channel scheme implies, however, that the GPe units project back only to the STN units in the same channel.

We now turn to the determination of the number of neurons in each channel. In real neural tissue, each neuron is innervated by up to several thousand axon collaterals. Clearly, this is difficult to replicate in a model and so we seek to understand how we might work with fewer synaptic inputs. In general, it may appear that if we halve the number of afferents, but double the synaptic weight of each afferent, then no loss in realism ensues. However, because the afferent spike trains exert a noisy and discontinuous influence, their combined affect is non-linear. To determine the smallest number of afferents that we could use, without significant loss in the transfer characteristics of the neurons, we ran a series of experiments with different numbers of inputs N into a single model neuron described by Eq. (6). Every input was a spike train generated using a binomial distribution. The results are shown in Table 1. Each column indicates, for each value of N, the output (in Hertz) of the neuron in response to different mean firing rates of the input spike trains. The final column shows the control case with 192 inputs and a weight c of 1. The outputs of this neuron were used as the target values for all subsequent experiments with smaller N values to determine if the corresponding increase in weight then led to a significant difference in output. It is clear from these results that small numbers of inputs (with correspondingly large weights) incur a loss in faithful reproduction of the control neuron's output, which is especially severe at high input firing rates. On the other hand, no gain in accuracy was found above $N = 16$ inputs and so we used 16 units per channel. We modelled only two channels because this was sufficient to observe the inter-channel interactions.

2.3.1. STN axon collaterals

Fujimoto and Kita (1993) have provided indirect evidence for extensive axon collateralisation in the STN. Furthermore, a recent study (Atherton, Gillies & Arbuthnott, 2000) has demonstrated that a glutamate antagonist can influence STN neuron firing patterns in a slice preparation where all external inputs to STN have been removed, thereby implicating glutamatergic intra-nucleus collaterals. It has been estimated that every STN neuron is, at most, two synapses away from every other STN neuron via its intra-nuclear axon collaterals (Gillies & Willshaw, 1998). This implies that an STN neuron has direct synaptic contact, via its axon collaterals, with approximately 25% of all STN neurons. In our network, to model the intra-nucleus connections in STN, each unit is, therefore, randomly connected to 25% of all other STN units both within and between channels. Thus, our model's STN is massively interconnected.

Recent modelling work (Gillies, Atherton & Arbuthnott, 2000) has indicated that an excitatory post-synaptic potential (EPSP) elicited by one STN neuron contacting another is likely to be small. Hence, a large number of coincident STN collateral induced EPSPs would be necessary for an STN neuron to depolarise sufficiently to release an action potential. In keeping with this data the weight c_{ss}^{+} of the STN–STN connections in normally functioning networks is kept relatively small (about 10% of the magnitude of other weights—see Table 2).

Table 2
Model parameter values

Parameter	Value
c_{ss}^{+}	1.2
c_{sg}^{+}	9.6
c_{gs}^{-}	−12
c_{cs}^{+}	12
J_{prox}^{*}	72
J_{soma}^{*}	60
C	2 μF
τ_m	70 ms
τ_s	3 ms
θ	30 mv
α_{Ca}	7.5 μA
θ_{Ca}	−10 mv
t_1	200 ms
t_2	1000 ms
I_{spon}	0.8 μA

2.3.2. Cortical input

Plenz and Kitai's (1999) data on bursting frequencies showed that the presence of one of their main burst frequencies (0.4 Hz) was dependent on there being cortical innervation of STN. Since there is no sensory input in vitro this implies that the spontaneous output of cortex was sufficient to cause this change in behaviour. To model cortical input to the STN, each STN unit was innervated with 16 spike trains that represent spontaneous cortical firing. This number is consistent with the number of neurons in a basal ganglia channel and with the extensive cortical innervation of STN (Bevan et al., 1995). Each spike train was generated using a binomial distribution (using Bernoulli trials at each time step of the simulation) modified to take account of a cortical absolute refractory period; thus, no two action potential spikes could be separated by less than 2 ms. While random neural spike trains are believed to follow a Poisson distribution (Segundo, Stiber & Vibert, 1995) it is also the case that the Poisson distribution approximates the binomial distribution when the chance of a trial success is small and a large number of trials are conducted (Ross, 1985). This approximation holds in our case, since the mean firing rate of each cortical input to STN was set at 4 Hz.

2.4. Analysis of simulation data

The purpose of the analysis is to characterise the bursting behaviour of individual units and pairs of units. In particular, we wish to know what units are bursting and, if they are, whether this bursting is phase locked with other units. Where result sets required extra analysis tools, these are detailed in the appropriate parts of Section 3.

Inter-spike interval (ISI) data were calculated from the spike-train of each unit. The ISI data were then sampled in 50 ms bins and the mean firing rate in each bin determined. The mean, or DC, component of each resulting signal was then subtracted before performing a power-spectral density (PSD) analysis. Each PSD analysis used a Hanning window with width equal to half the number of bins (e.g. in a $T = 60$ s simulation with 50 ms bins the Hanning window had a width of 600). The PSD analyses were high-pass filtered at 0.07 Hz to remove window edge-effects. Each unit was then assigned a fundamental frequency f_0 which was the frequency associated with the largest power in the PSD.

f_0 is, putatively, the frequency of bursting, but determination of bursting status requires more work. The starting point for this analysis is the computation of the unit's autocorrelogram (ACF) (after extraction of the DC component). The ACF always contains an oscillatory component that corresponds to f_0 and the depth of modulation of this component is an indication of the power present in the original signal at this frequency. We, therefore, used this feature to determine if a unit was bursting. To quantify this, let the ACF functional form be denoted by $A(t)$. $A(t)$ is symmetric about $t = 0$ at which point it takes its maximum value. Let $\tau_0 = 1/f_0$ (the fundamental period of the unit). To be sure of inspecting a full period τ_0 we examined $A(t)$ over the (half-open) interval $\Delta t = (0,\ 3\tau_0/2)$. Let $a_{max} = \max_{\Delta t}(A(t))$, $a_{min} = \min_{\Delta t}(A(t))$ and $d = |a_{max} - a_{min}|$. The quantity d is therefore a measure of the depth of modulation of the ACF at f_0. Now, fix a threshold ratio θ_a; then the unit was deemed to be bursting if

$$d > \theta_a A(0) \tag{15}$$

We chose θ_a by ensuring that units that were clearly bursting in one of our simulations (by direct visual inspection of their ISI data) were assigned the bursting status according to Eq. (15); this gave a value $\theta_a = 0.2$.

We now go on to describe our methods for determining the presence of bursting synchrony. Candidates for burst synchrony are drawn from all STN–STN, GPe–GPe and STN–GPe pairs for which both units in the pair satisfy Eq. (15). To determine if a pair is synchronised (phase locked) we compute a *synchrony index* S as follows. Let f_0^1, f_0^2 be the fundamental frequencies of the two units. Express these as integral multiples n_0^1, n_0^2 of the smallest frequency expressible in the analysis (this is just the frequency step in the PSD which is, in turn, fixed by the Hanning window size and the bin size of the original ISI data). Let N_{12} be the least common multiple (lcm) of n_0^1 and n_0^2. Then, the signals are coincident every N_{12}/n_0^2 periods of signal 1 and N_{12}/n_0^1 periods of signal 2. High degrees of synchrony are, therefore, associated with small values of these quantities or, alternatively, large values of their reciprocals. We, therefore, define S to be the mean of these two latter quantities

$$S = \frac{n_0^1 + n_0^2}{2N_{12}} \tag{16}$$

where $0 < S \leq 1$. To clarify our understanding of this definition we now consider two examples. First, we suppose that identical signals constitute the case of maximal synchrony,

which is consistent with their giving $S = 1$. Second, consider the case of two signals which differ slightly in frequency and for which $N_{12} = n_0^1 n_0^2 \approx n_0^{12}$. In this case, $S \approx 1/2n_0^1$, which tends to zero as n_0^1 becomes very large. This is consistent with the idea that two signals which have slightly differing frequencies are probably not causally related and should not, therefore, be considered as phase locked.

To explore phase angles in synchronous signal pairs, we first take the cross spectral density analysis (CSD) of the pair (after DC subtraction) to determine the common frequency of firing of both units, f_0^c, and its associated period τ_0^c. Next, we compute the cross correlogram (CCF) (after DC subtraction) and denote its functional form by $C(t)$. This function is, in general, not symmetric about zero and has a maximum value $C(t_{max})$ where (again in general) $t_{max} \neq 0$. t_{max} is the relative time displacement that the two signals have to undergo in order to find their largest overlap. We now convert this into a phase difference ϕ_{max} with respect to f_0^c according to

$$\phi_{max} = 360 \frac{t_{max}}{\tau_0^c} \tag{17}$$

All pairs that gave $\phi_{max} > 360$ were excluded as the occurrence of phase angles greater than 360° implies a group of bursts in each signal which is not temporally coincident with its counterpart.

2.5. Implementation details

The equations for the membrane potentials of GPe and STN units were solved in a discrete time simulation with a fixed time interval of 0.1 ms. This was the largest interval commensurate with accurate solution over a wide range of conditions. For all the simulations described below, noise (the I_{noise} component) was sampled at each time step from a Gaussian distribution ($\bar{x} = 0, \sigma^2 = 0.5$). The simulation was written in Matlab v5.2.

3. Results

The parameters for all the simulations described below, and their normal values, are listed in Table 2. Some of these parameters were not relevant to or were varied for some simulations. These are detailed in the appropriate cases. In every simulation the GPe neurons were described by Eq. (6).

3.1. STN neuron-like bursting is not possible without the Ca^{2+} mechanism

One of the primary hypotheses of this paper is that the Ca^{2+} mechanism described by Beurrier et al. (1999) was crucial in causing the bursting behaviour of STN neurons observed by Plenz and Kitai (1999). Hence, we would expect that the STN–GPe circuit, without the Ca^{2+} mechanism in place, would not be capable of showing neurophysiologically realistic bursting behaviour. This is not self evident, as it has been demonstrated that a simple central pattern generator (CPG) circuit, consisting of two reciprocally linked excitatory units, can exhibit synchronised bursting behaviour when neither of the units is an endogenous burster (Rowat & Selverston, 1997). Bursting within this CPG was dependent upon either the units having heterogeneous firing thresholds, or on the units receiving significantly different amounts of injection current. In short, bursting was caused by a breaking of the symmetry between the two units.

These findings are directly relevant to the network discussed here, as the reciprocal excitatory connections between STN units set up just such a circuit in which two mutually excitatory units may be receiving different levels of input (from GPe units and other STN axon collaterals). Furthermore, the noise introduced by the $I_{noise}(t)$ current is equivalent to a noisy threshold (Gerstner, 1999). Hence, any two units will effectively have different firing thresholds at any particular time step. Thus, any mutually connected pair of STN units may have their symmetry broken sufficiently to allow bursting to occur.

To test the possibility that STN units could be induced to burst without a Ca^{2+} mechanism, three simulations were conducted using an STN–GPe network in which STN model neurons were described by Eq. (7) and in which c_{ss}^+ took the values of 1.2, 6 and 12. This was done to ascertain if any level of axon collateral connection strength could induce bursting. All other relevant parameters had the values shown in Table 2. There was no external input to the network.

Fig. 4(a) shows the binned ISI plot of an example STN from the simulation with $c_{ss}^+ = 1.2$. STN units from the other two simulations showed qualitatively the same results. The narrow peaks of mean firing rate coincide with pairs or triples of spikes that are close together in time (Fig. 4(d)).

The binned ISI plot and spike train for a typical STN bursting neuron from Plenz and Kitai's study are shown in Fig. 4(c) and (f). A comparison of these data with the binned ISI plot and spike train from the example STN unit shows that these units were not bursting in the same manner as real STN neurons.

It seems, then, that it is not possible to induce STN neuron-like bursting in this network without the addition of the Ca^{2+} mechanism to the STN units. However, within the literature on thalamic neuron rebound bursting, authors have reported bursts that consist of as few as two spikes (Ulrich & Huguenard, 1997) and which have a normal range of five–15 spikes (Kim & McCormick, 1998; Kim, Sanchez-Vives & McCormick, 1997). Furthermore, authors rarely report the incidence of more than one burst. Their criteria for what constitutes a burst can, therefore, be characterised as: action potentials must occur closely in time; as few as two action potentials are enough to define a burst; and the absence of repeated occurrences of groups of action potentials does not exclude a neuron from being classified as

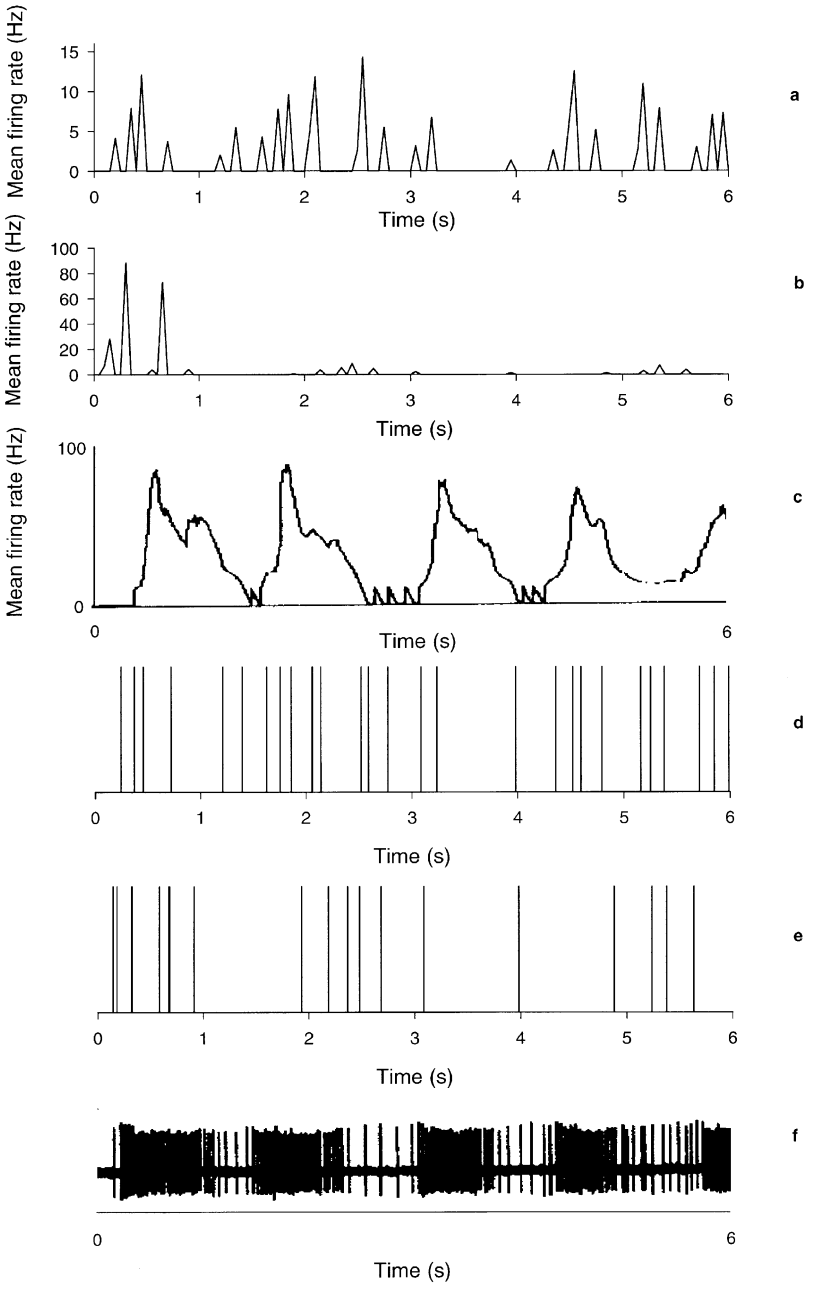

Fig. 4. STN units could not burst-fire without the Ca^{2+} mechanism. (a)–(c) Binned ISI plots determined from the spike trains in (d)–(f), respectively. (a) An example STN unit from a simulation with $c_{ss}^{+} = 1.2$. It shows very short bursts of firing at an intra-burst maximum of 15 Hz. (b) ISI plot of a spike train generated by a Poisson process. (c) A bursting STN neuron from Plenz and Kitai's (1999) study. (d) The spike train of the simulated STN unit. The close incidence of a few spikes, for example at $t = 2$ s, caused short bursts to appear in the binned-ISI plot. (e) Spike train generated according to a Poisson process. (f) Spike train of the bursting STN neuron from Plenz and Kitai's study. It is clear that the simulated STN unit was not bursting in qualitatively the same way as the typical bursting STN neuron, but was similar to a randomly generated output. Figures reprinted by permission from *Nature* (*400*:677) copyright (1999) Macmillan Magazines Ltd.

bursting. Similar criteria to these have been used for studies of bursting neurons in other areas of the mammalian brain (White, Lovinger & Weight, 1989). Hence, according to these criteria, it is possible to interpret the binned ISI plot and spike train of the example STN unit as showing bursting.

However, the example STN unit's spike train is similar to a spike train obeying a Poisson distribution. This is illustrated by the train in Fig. 4(e) which was generated according to a Poisson distribution. The corresponding binned ISI plot is shown in Fig. 4(b). Hence, even though it is possible to interpret the example STN unit's data as showing bursting, the similarity between these data and the data generated according to a Poisson distribution indicates that there is no underlying mechanism causing this bursting, because it is indistinguishable from a randomly generated example.

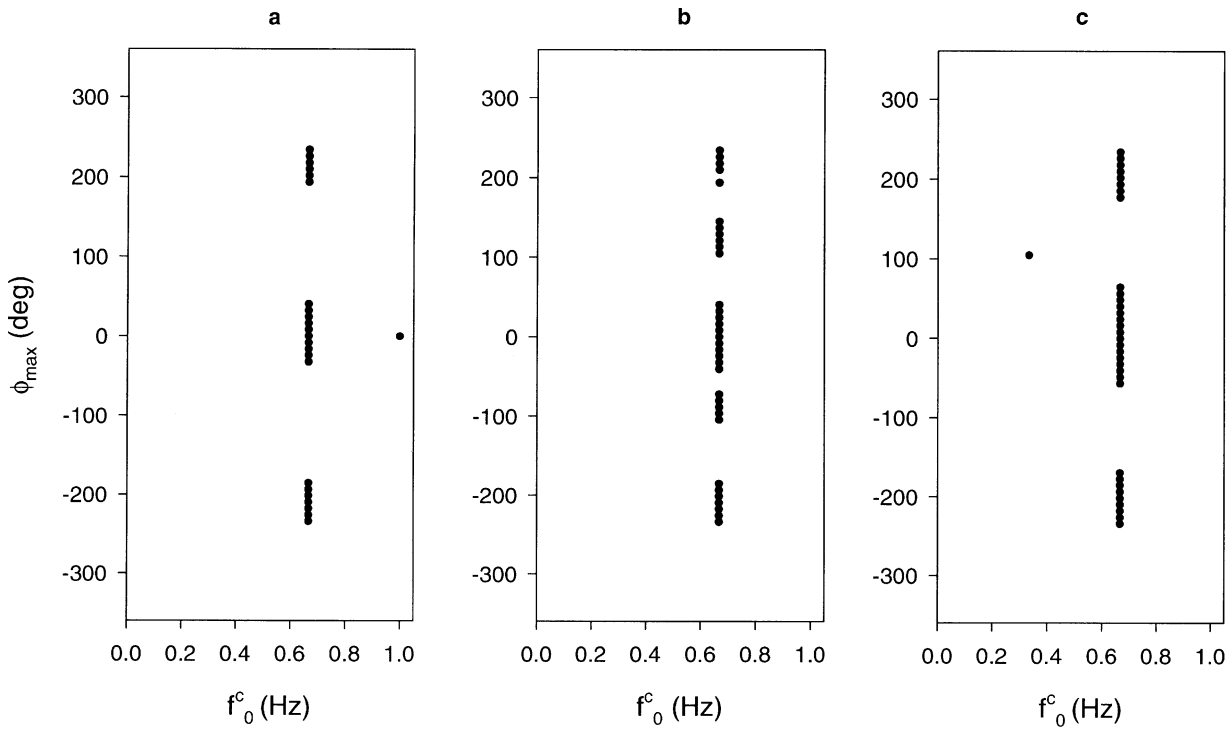

Fig. 5. Phase angle (ϕ_{max}) plots for STN unit pairs in three simulations of Experiment 2 with $c_{ss}^{+} = 1.2$ (a), 6 (b) and 12 (c), respectively. Almost all units had a common frequency of firing at 0.67 Hz, regardless of the level of c_{ss}^{+}, and all had similarly wide ranges of ϕ_{max} indicating that most units were out-of-phase with each other.

3.2. The role of noise

Having shown that neurophysiologically realistic STN bursting was not possible without the Ca^{2+} mechanism, it remained to be shown that the addition of this mechanism to the model neuron would cause bursting in STN units within a network. In this section we used the model neuron described by Eq. (9) for all STN units, with the parameters from Table 2 (except where explicitly stated below). Again, there were no external inputs to the network. Four experiments were carried out as described below. The first two experiments confirmed that the addition of the Ca^{2+} mechanism caused bursting to occur. The other two experiments investigated the affect of removing noise from the network.

3.2.1. Experiment 1

A simulation of the STN–GPe network without intra-nucleus axon collaterals within STN (a 'collateral-free' network, with $c_{ss}^{+} = 0$) showed that units equipped with the Ca^{2+} mechanism were able to burst when placed in a network. The burst detection algorithm found that all units burst. f_0 for all units was 0.67 Hz indicating that the network was bursting mono-modally. The cross-spectral density analysis showed that the common frequency, f_0^c, between all bursting unit pairs was also 0.67 Hz. The mean synchrony index S was 0.982. The breakdown of this value into its constituent mean scores from STN unit pairs (S_{ss}), GPe unit pairs (S_{gg}), and STN–GPe unit pairs (S_{sg}) was: $S_{ss} = 0.982$; $S_{gg} = 1$; and $S_{sg} = 0.964$. The S scores show that the vast majority of units were completely phase locked within STN and GPe and across both nuclei.

3.2.2. Experiment 2

Three simulations, with c_{ss}^{+} values of 1.2, 6 and 12, of the network with axon collaterals within STN were run. The results were very similar to those of Experiment 1 for all c_{ss}^{+} values. f_0 for every unit in each of the simulations was 0.67 Hz. f_0^c for almost all bursting pairs was also 0.67 Hz. The phase angle plots in Fig. 5(a)– (c) show that the variation of ϕ_{max} was consistent in all three simulations and, hence, did not change with increasing c_{ss}^{+}.

3.2.3. Experiment 3

To investigate how the presence of noise affects the network's behaviour, three simulations were run with the same parameters as those in Experiment 2, except that I_{noise} was set to zero. All three simulations showed burst firing in all units. Again, f_0 was 0.67 Hz for all three values of c_{ss}^{+}. The phase angle plots for STN unit pairs are shown in Fig. 6. It is immediately apparent that with increasing c_{ss}^{+} came an increasingly diverse data set: the variation of ϕ_{max} increased going from $c_{ss}^{+} = 1.2$ to $c_{ss}^{+} = 6$, and at $c_{ss}^{+} = 12$ a third f_0^c was observed. This is in direct contrast to the results of the equivalent simulations with noise, reported in Experiment 2, and suggests that noise acts to homogenise the behaviour of units in the network.

This suggestion is supported by the mean S scores from

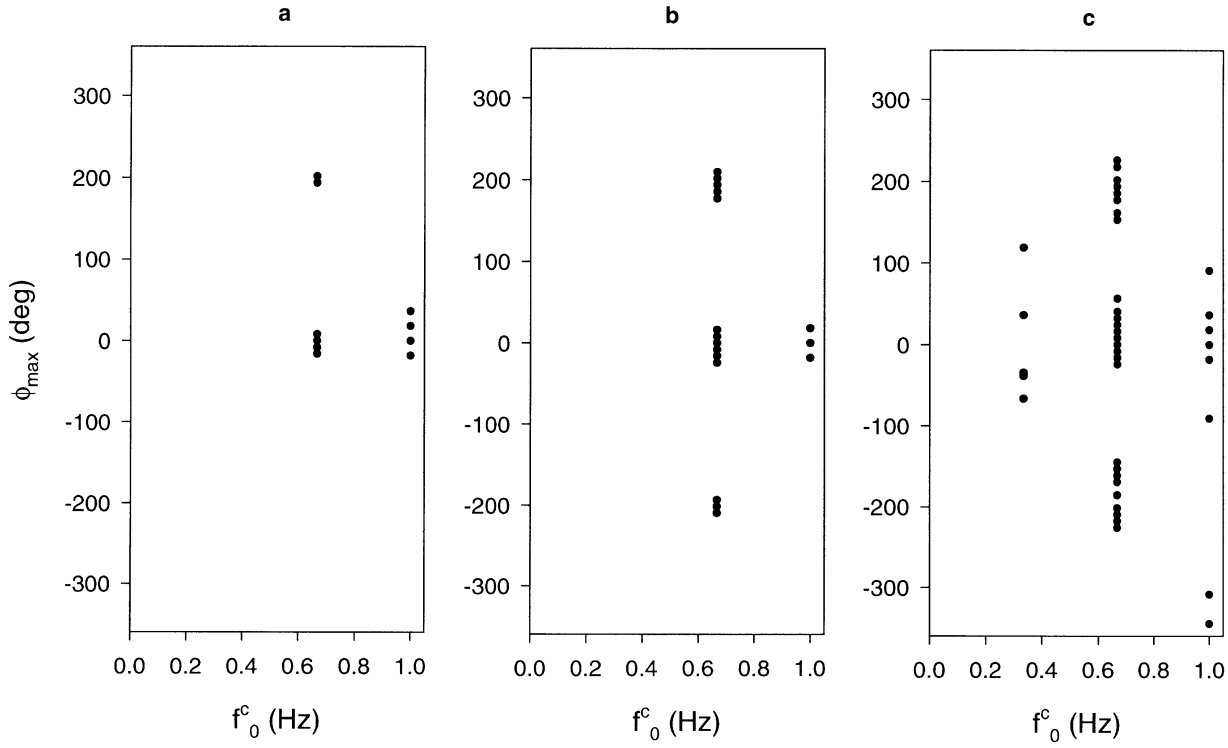

Fig. 6. The phase angle plots of STN bursting unit pairs for three simulations from Experiment 3, with $c_{ss}^{+} = 1.2$ (a), 6 (b) and 12 (c), respectively. The phase angle plots showed that increasing c_{ss}^{+} caused a diversification of the data set: a wider range of ϕ_{max} and a third common frequency of firing between pairs of units.

Experiments 2 and 3. These are broken down in Table 3 for all six simulations (three with noise, three without). The mean S scores show that STN–GPe unit pairs and STN unit pairs became less phase locked when noise was removed from the network. The presence or absence of noise in the network did not affect the degree of phase locking in GPe unit pairs. Hence, the S scores show that removing noise reduces the level of synchrony in the STN–GPe circuit.

3.2.4. Experiment 4

A simulation of the collateral-free network used in Experiment 1 (i.e. with $c_{ss}^{+} = 0$), but with I_{noise} set to zero, showed no firing in any unit. Clearly, the removal of noise meant that the membrane potential in STN units never reached θ. Thus, no STN output ensued with which to drive GPe units. This, in turn, meant that there was no inhibition from GPe to STN units with which to cause bursting.

To establish if a collateral-free network with no noise could ever burst fire, we ran two simulations of the same network with higher values of I_{spon} (3 and 5) than the default value in Table 2. Increasing I_{spon} increases STN unit output and, therefore, would cause greater GPe inhibitory feedback. This would, in turn, hyperpolarise the membrane of the STN units more than in the initial simulation with the default value of I_{spon} and, possibly, reach the level of θ_{Ca}.

All STN units in the two simulations had similar outputs: an initial burst was followed by persistent tonic firing. The bursting detection algorithm confirmed that no units in STN or GPe were bursting in either simulation. This indicates that removing noise in a collateral-free network prevents the STN units from burst-firing, regardless of the level of input they provide to GPe units.

Table 3
Mean S scores for Experiments 2 and 3 ('noise' and 'no noise')

$S_{unit\text{-}pair}$	c_{ss}^{+}					
	Noise			No noise		
	1.2	6	12	1.2	6	12
S_{ss}	0.964	1	1	0.757	0.898	0.789
S_{gg}	1	1	1	1	1	1
S_{sg}	1	1	1	0.931	0.931	0.931
$\bar{x}S$	0.979	1	1	0.896	0.943	0.907

3.3. Simulation of the basal ganglia pacemaker

Having established that the Ca^{2+} mechanism could cause burst firing of units in a network, it remained to be shown that the multi-frequency bursting observed by Plenz and Kitai could be simulated. The results of the previous section showed that the model neuron described by Eq. (9) was capable of mono-modal bursting, at 0.67 Hz, when placed in a network. One of our primary hypotheses is that cortical input will modulate the intrinsic bursting properties of the

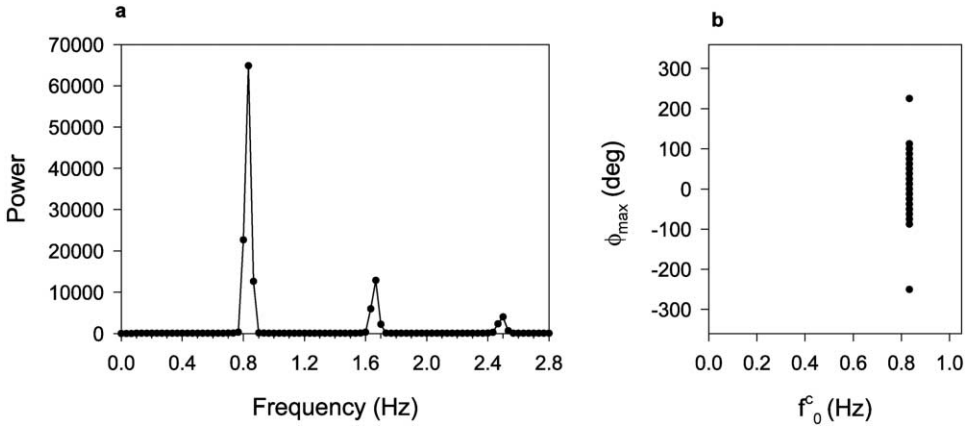

Fig. 7. (a) The mean power-spectral density analysis of all bursting units in a simulation of the network with quasi-compartmental model neurons (Experiment 5). The main frequency of bursting was 0.82 Hz. (b) The phase angle plot for STN unit pairs shows a wide range of ϕ_{max} indicating that most phase locked units were out-of-phase with each other.

STN–GPe circuit and cause multiple frequency bursting. To test this hypothesis we introduced cortical input, as described in Section 2.3.2, to a network with STN axon collaterals using the model neuron described by Eq. (9) for STN units. The parameters were set as shown in Table 2.

Results from a simulation of this network indicate that cortical input was not sufficient to cause multiple frequency bursting in the STN–GPe network. The fundamental frequency f_0 for all units was 0.77 Hz and, hence, so too was the frequency of bursting (the bursting algorithm found that all units burst). No other frequencies were evident from the PSD and CSD analyses.

We then tested networks which used the quasi-compartmental model neuron in the STN, described by Eq. (14). The parameters used are those in Table 2.

3.3.1. Experiment 5

A simulation of 60 s duration was run without cortical input to attempt to repeat the mono-modal bursting already achieved by the network in Experiments 1 and 2. Fig. 7(a) shows the mean PSD analysis for all bursting units. From the PSD analysis it is evident that the only frequency of firing of any significance is 0.82 Hz ($p(f_0 = 0.82) = 1$). The burst detection algorithm found all units were bursting. Hence, without cortical input, STN and GPe quasi-compartmental units burst fire at ~0.8 Hz which is in good agreement with the results observed by Plenz and Kitai (1999) in their cortex-disconnected condition.

The phase angle plot in Fig. 7(b) shows that STN unit pairs had a wide range of ϕ_{max} indicating that, although the majority were phase locked ($S = 0.94$), they were normally out-of-phase with each other. Phase locked GPe unit pairs showed complete synchrony ($S = 1$) with $\phi_{max} = 0°$ indicating that all units were completely in-phase.

3.3.2. Experiment 6

To investigate the effects of cortical input on the network's behaviour, three simulations of 60 s duration were run, with cortical input as described in Section 2.3.2. This was done to gather a large data set: it was evident from the first simulation that the data set was very rich and that we needed a larger population of units to establish results. Hence, the total number of units in the results outlined below is 192 (96 STN and 96 GPe units).

For the analysis of this data set we used 100 ms bins. Increasing the bin size acts as a low-pass filter because the maximum frequency f_{max} that can be detected is determined by

$$n = \frac{1}{s} \tag{18}$$

$$f_{max} = \frac{n}{2}$$

where s is bin size in seconds, and n is the number of bins in 1 s. Therefore, as bin size increases, the maximum frequency that can be detected decreases, with 100 ms bins, $n = 10$ and $f_{max} = 5$ Hz. We used 100 ms bins to low-pass filter the GPe data because the power-spectral density analyses showed a significant amount of power at high frequencies which obscured any low frequency bursting. To enable cross-nucleus analysis (cross-correlograms, cross-spectral density analyses and phase angle plots) the STN data were also binned at 100 ms. However, we also binned all the STN data at 50 ms for comparison purposes and the within-nucleus analyses (power-spectral density analyses, autocorrelograms, STN–STN phase angles) were identical to those shown here.

Fig 8(a) shows the mean power-spectral density analysis for all bursting units. It reveals that bursting occurred at two main frequencies $f_{01} = 0.67$ Hz and $f_{02} = 0.83$ Hz. The largest mean PSD analysis peak was at f_{02} indicating that it was the dominant bursting frequency. The mean PSD analysis from Plenz and Kitai (1999) is shown in Fig. 8(b).

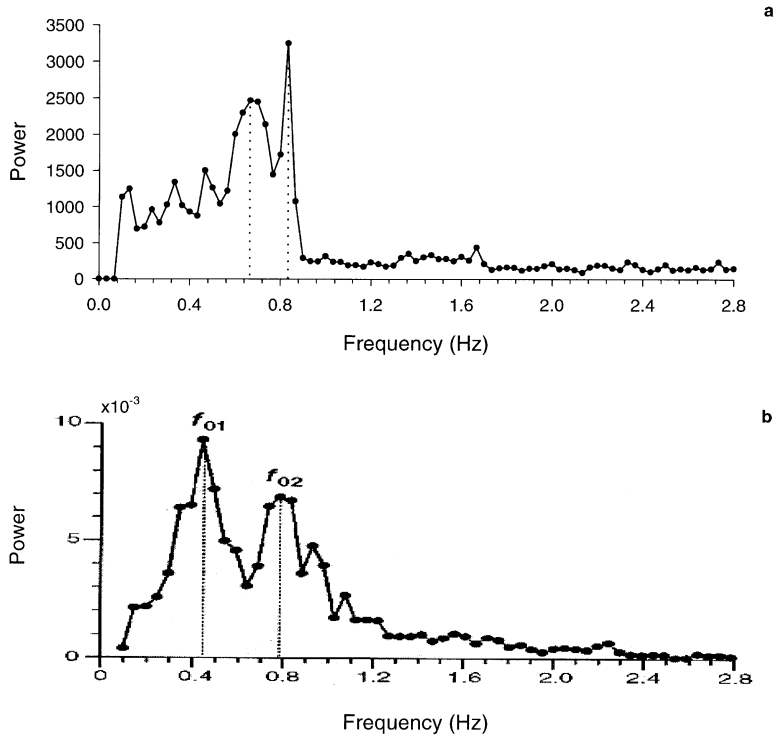

Fig. 8. (a) Mean PSD analysis of all bursting units from three simulations of the STN–GPe network of quasi-compartmental units which received cortical input (Experiment 6). The dominant frequencies were 0.67 and 0.83 Hz. (b) The equivalent mean power-spectrum analysis from Plenz and Kitai's (1999) study showing two main frequencies of 0.4 and 0.8 Hz. Figure reprinted by permission from *Nature* (*400*:677) copyright (1999) Macmillan Magazines Ltd.

It clearly illustrates two peaks at ~0.4 and ~0.8 Hz, which they reported as the dominant bursting frequencies, and is qualitatively similar to our mean PDS analysis.

The bursting algorithm returned 101/192 (101 out of 192 units tested) units as bursting (69/96 STN units, 32/96 GPe units). Plenz and Kitai reported similar proportions of bursting neurons in these nuclei: 83/181 bursting STN neurons and 31/102 bursting GPe neurons.

The mean cross-spectral density analysis of all bursting pairs (STN–STN, STN–GPe and GPe–GPe) is shown in Fig. 9(a). Again, there were two main frequencies, $f_{01} = 0.63$ Hz and $f_{02} = 0.8$ Hz which were very close to those found in the mean PSD analysis. However, in contrast to the mean PSD analysis, the lower frequency (f_{01}) dominated. Again, for comparison purposes, the mean PSD analysis from Plenz and Kitai (1999) is shown in Fig. 9(b): note that the greater power is at the lower peak in both spectra.

Phase angle plots of STN unit pairs and GPe unit pairs are shown in Fig. 10. The phase angle plot for the STN unit pairs clearly shows that synchronised firing was not limited to a single f_0^c. STN unit pairs showed the closest phase of bursting when their common frequency, f_0^c, was low. This degree of phase diversified with increasing f_0^c so that the most out-of-phase pairs were those with $f_0^c = \sim 0.8$ Hz. Phase locked GPe unit pairs were in complete synchrony at all f_0^c ($\phi_{max} = 0$). The mean S was 0.449 indicating that many unit pairs were not phase locked. A comparison of the phase angle plots with their equivalents from the no-cortical input network (in Fig. 7(b)) shows that the introduction of cortical input caused a substantial diversification of unit outputs.

The example binned ISI plots in Fig. 11(a)–(c) illustrate the range of STN unit behaviour: non-bursting units, which showed rapidly oscillating high frequency tonic firing, sporadically bursting units, and regularly bursting units. Fig. 11(e) shows binned ISI data, taken from Plenz and Kitai's study, for an STN neuron bursting at 0.8 Hz. A comparison of these data with the 0.8 Hz bursting unit in Fig. 11(d) shows that both had a maximum intra-burst firing rate of ~100 Hz and had alternating periods of quiet and low-level tonic firing between bursts.

Fig. 12 shows example STN unit spike trains from the cortical and no-cortical input simulations and equivalent spike trains from Plenz and Kitai's study. The STN neuron spike train from a cortex-intact culture (Aa) shows long bursts with short inter-burst quiet periods often interrupted by occasional spikes. The STN neuron spike train from the cortex disconnected culture (Ab) shows very short bursts with long, completely silent, inter-burst periods. The example STN unit spike trains from the cortical and no-cortical input simulations (Ba and Bb, respectively) show that our model neuron can emulate these real phenomena very well.

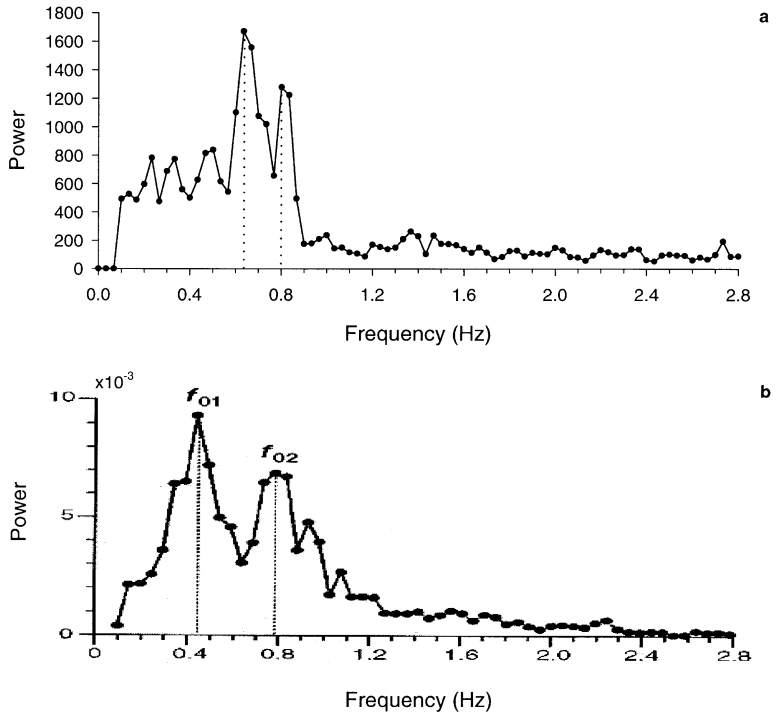

Fig. 9. (a) The mean CSD analysis of all bursting unit pairs from the three simulations of the network with quasi-compartmental units and cortical input. The main peaks are at 0.8 and 0.63 Hz. These were similar frequencies to the mean analysis in Fig. 8(a), but the main power was at the lower frequency in this case. (b) The mean power-spectrum analysis from Plenz and Kitai's (1999) study showing the greatest power at the lowest peak (0.4 Hz). Figure reprinted by permission from *Nature* (*400*:677) copyright (1999) Macmillan Magazines Ltd.

4. Discussion

4.1. Ca^{2+} is essential for bursting

The results from Section 3.1 showed that neurophysiologically realistic STN neuron bursting could not be achieved by the STN–GPe network without the Ca^{2+} mechanism within the STN model neurons. Moreover, even though it was possible to interpret the STN model neuron outputs as bursting, according to criteria set out by researchers of

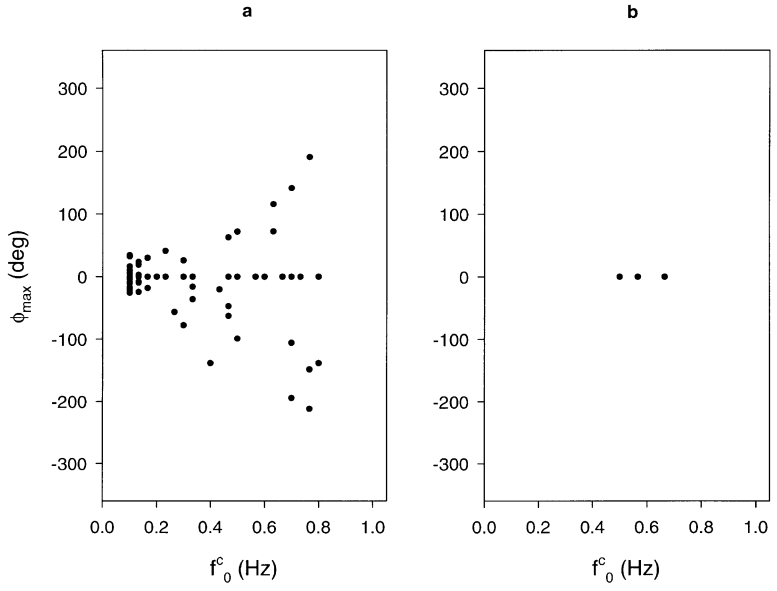

Fig. 10. The phase angle plots for all bursting STN (a) and GPe (b) unit pairs from Experiment 6. STN unit pairs showed a wide range of ϕ_{max}: at low f_0^c the unit pairs were bursting in-phase; at higher f_0^c unit pairs were substantially more out-of-phase. The clustering of ϕ_{max} at zero indicates that all phase locked GPe units burst in phase.

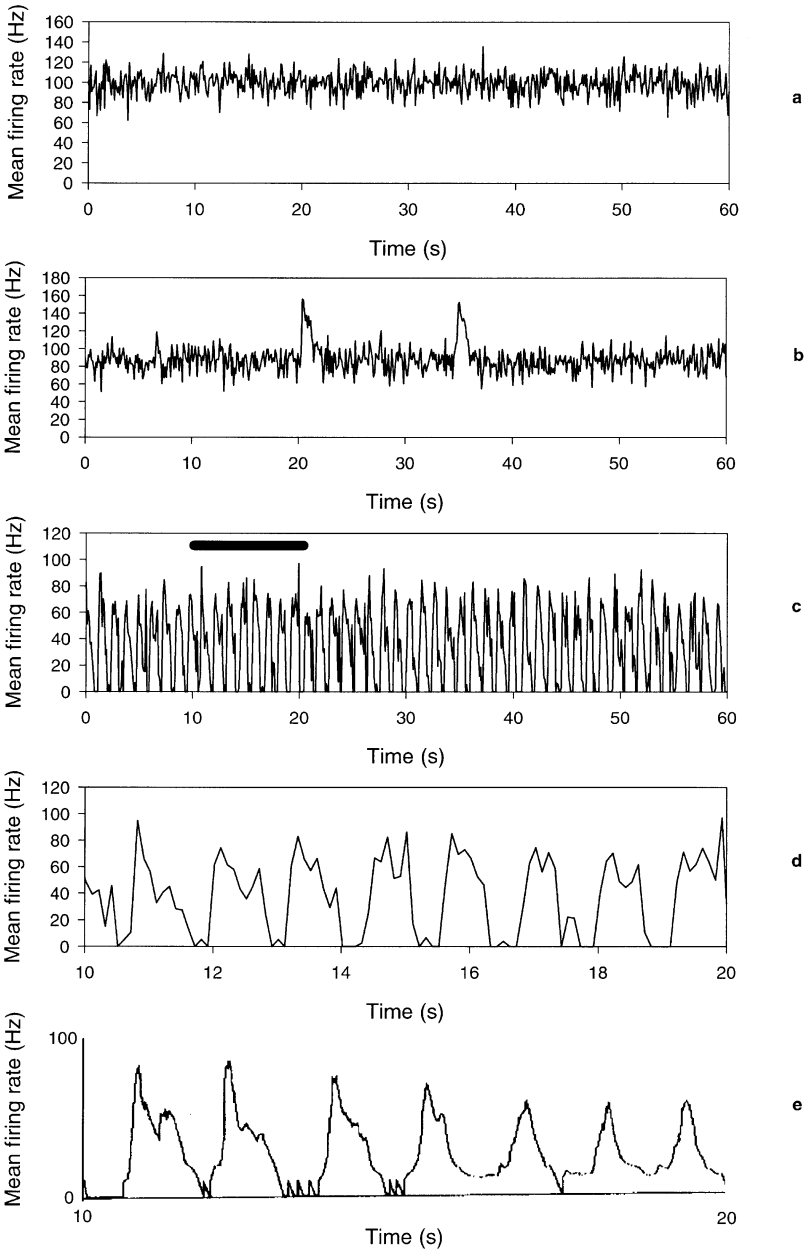

Fig. 11. Example binned ISI plots from STN units showing noisy tonic firing (a), sporadic bursting (b) and regular 0.8 Hz bursting (c). The heavy black bar indicates the section enlarged in (d). An equivalent section from a 0.8 Hz bursting STN neuron from Plenz and Kitai's study is shown in (e). They both show a maximum intra-burst firing rate of 100 Hz and occasional quiet inter-burst periods. Figures reprinted by permission from *Nature* (*400*:677) copyright Macmillan Magazines Ltd.

thalamic neuron rebound bursting, this does not provide any support for Rowat and Selverston's (1997) findings (which were outlined in Section 3.1). This was because the spike trains of the STN units were similar to those generated by a Poisson distribution and, therefore, there was no underlying mechanism causing this bursting. Instead, the probable source of the bursting observed was the noise component, I_{noise}, of the membrane equation: a short period of high-level, positive noise would cause a few spikes to be fired consecutively at short intervals giving the appearance of 'bursting'.

4.2. The affects of noise

One affect of noise on a model neuron's output is clear: without noise all model neurons, with the same parameters, would give identical outputs. However, we have found that noise interacts with the extended spiking model neuron in a non-intuitive manner.

In a noise-free network, with no STN axon collaterals, no units could be made to burst fire regardless of the level of I_{spon}. Hence, noise is essential for bursting in a collateral-

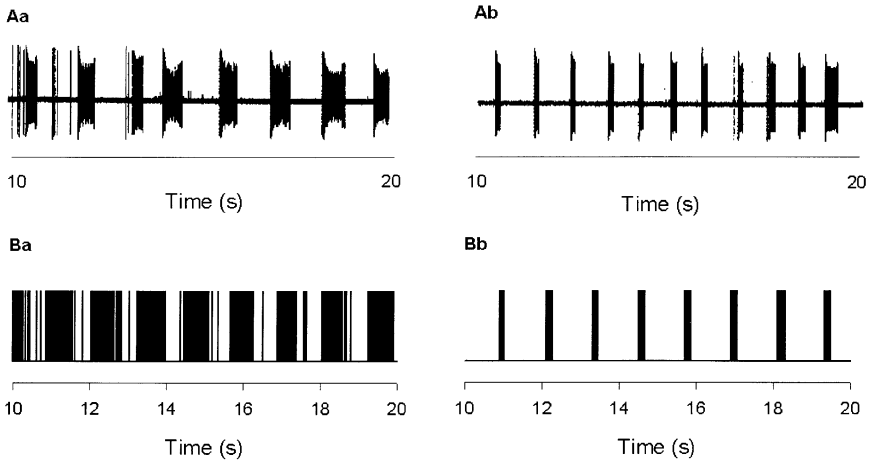

Fig. 12. Aa, Ab example STN neuron spike trains for the cortex-intact and cortex-disconnected conditions, respectively, from Plenz and Kitai's study. Ba, Bb example STN unit spike trains from the corresponding network simulations with cortical input and without cortical input, respectively. The study data and simulation data are qualitatively similar. Figures reprinted by permission from *Nature* (*400*:677) copyright (1999) Macmillan Magazines Ltd.

free STN–GPe circuit. By contrast, in a noise-free network with axon collaterals within the STN, burst firing still occurred. Furthermore, we also found that increasing c_{ss}^{+} in a noise-free network caused unit outputs to diversify. An identical network, but with noise, showed a very homogeneous data set regardless of the value of c_{ss}^{+}. The conclusion we draw from these results is that, paradoxically, the introduction of noise to the network acted to decrease the disorder of the network's behaviour.

The ability of STN units to burst fire in a noise-free network is wholly dependent on the presence of intra-nucleus axon collaterals. Because the collaterals from each STN unit are randomly connected to 25% of all other STN units, each unit receives a different set of STN axon collateral inputs. Hence, some STN units will receive greater excitation than others because they have a greater number of collateral inputs. Since all GPe units receive input from every STN unit, these would be driven harder in a network equipped with STN collaterals than in a collateral-free network. This, in turn, would cause greater GPe firing, which would be sufficient to hyperpolarise the STN units with less excitation and cause them to burst. Hence, the presence of axon collaterals introduces what may be termed 'structural' noise which may play the same role as the I_{noise} current component.

4.3. Quasi-compartmental modelling

4.3.1. The use of Plenz and Kitai's study

We have focused on Plenz and Kitai's study primarily because we used their data as a test-bed for our modelling approach: the phenomenological replication of each additional contribution to the membrane potential and a simple replication of synapse distribution. In this regard, their study was ideal because of the highly controlled nature of the culture which allowed a close comparison with a limited circuit model. Furthermore, the frequencies of bursting they observed are slow enough to be relevant at a behavioural level. This is of particular interest to us as part of our wider computational study of the involvement of the basal ganglia in action selection (Gurney et al., 2001a,b; Humphries & Gurney, 1999; Redgrave et al., 1999).

Plenz and Kitai noted that their culture could be considered 'parkinsonian', due to the lack of dopamine, but we have not included any comparison between the network's performance and Parkinson's patient or animal model data. We felt that such data were not relevant because the culture was not strictly in a parkinsonian state for two important reasons. First, there is much neurophysiological evidence that suggests that the D2 dopamine receptors have an inhibitory affect on striatal neurons and the D2 equipped striatal neurons project predominantly to GPe (Delgado, Sierra, Querejeta, Valdiosera & Aceves, 2000; Gerfen & Wilson, 1996; Hsu, Huang, Yang & Gean, 1995). Therefore, under parkinsonian conditions, the lack of dopamine would increase the net inhibition of the GPe neurons by the D2-type striatal neurons, leading to a reduction in the firing rate of GPe neurons (Raz, Vaadia & Bergman, 2000). This could not occur in Plenz and Kitai's culture as cortical input was not sufficient to cause the striatal neurons to fire. Second, the main frequencies of oscillation/bursting found within a dopamine depleted basal ganglia are between 3 and 8 Hz (Bergman, Feingold, Nini, Raz, Solvin, Abeles et al., 1998; Bergman, Wichmann, Karmon & DeLong, 1994; Magnin, Morel & Jeanmonod, 2000), which correspond to the frequency range of resting tremor in MPTP-treated primates and Parkinson's patients. Nothing approaching these frequencies was found in the data from Plenz and Kitai's culture. Thus, we felt that comparisons between our network's performance and data from Parkinson's patients and animal models were inappropriate.

4.3.2. Qualitative simulation of Plenz and Kitai's data

We have demonstrated that an STN–GPe network, with

quasi-compartmental model neurons within STN and with cortical input, showed bursting at two main frequencies (~0.67 and ~0.83 Hz) in STN and GPe units. The same network without cortical input had only one bursting frequency at 0.82 Hz. This is qualitatively similar to the major result of Plenz and Kitai's study: there are two main frequencies of bursting with cortex-intact and only one with cortex-disconnected.

We also showed that other aspects of the simulation data compared favourably with the equivalent data from Plenz and Kitai's paper. The spike trains and binned ISI plots from the simulation data all had qualitatively similar properties to their equivalents derived from the neurophysiological data. The quasi-compartmental model network also showed some features that were not studied by Plenz and Kitai. Most significantly, we found that the addition of cortical input caused units to become less synchronised (in terms of the *S* values). Thus, we are able to make a prediction based on our model's results: subsequent neurophysiological studies or, possibly, a re-analysis of Plenz and Kitai's data will show that lesioning the cortex acts to increase the level of synchrony in the STN–GPe circuit.

The diversification of unit behaviour with cortical input, such as the multiple frequencies of bursting, was observed in both our simulations and in Plenz and Kitai's study. It can be attributed to the 'driving' of a non-linear system, the STN–GPe circuit, which is known to cause a bifurcation of these systems' modes of behaviour (Gaponov-Grekhov & Rabinovich, 1992): in the case of the STN–GPe network cortical input caused a bifurcation of bursting frequencies.

We did find, however, that there were two main discrepancies between our frequency data and Plenz and Kitai's. First, we found that the ~0.83 Hz frequency had the highest power-spectral density peak in both cortical and no-cortical input cases. Their data showed that, with cortical input, the lower of the two main frequencies (in their case 0.4 Hz, in ours ~0.67 Hz) was by far the most powerful. To determine the mean power spectrum (which they term the 'differential relative power spectrum'), from which they obtained their bursting frequencies, they averaged over power- and cross-spectral density analyses. We contend that this analysis possibly obscured the bursting frequencies of individual populations in the STN–GPe circuit because cross-spectral density analyses show the relative power in each of the possible *shared* frequencies of both types of neuron. This is plausible, as we found that the mean cross-spectral density analysis of our cortical input data clearly had the greater power at the lower main frequency (0.63 Hz); see Fig. 9. Hence, we would suggest that, without the inclusion of the paired unit frequency data, their spectral analyses may have shown the 0.8 Hz frequency as the dominant frequency in both cortex-intact and cortex-disconnected cases.

Second, the 0.4 and 0.8 Hz peaks found in the cortex-intact condition had a ratio of 0.5, whereas the power-spectral density peaks (0.67 and 0.83 Hz) from our network's data had a ratio of 0.81. The possible significance of the frequency ratio was not discussed by Plenz and Kitai. However, we believe it is possible, in principle, to obtain a mean power-spectral density peak at 0.4 Hz using our model. The data from Experiment 6 showed that the frequency of bursting for individual units ranged between 0.1 and 0.86 Hz with a small set of units bursting around 0.4 Hz (6/101 bursting units). Further exploration of the model parameters or the use of alternate formalisms for some aspects of the quasi-compartmental model (such as the shunting inhibition) may yield results with two main frequencies in a 0.5 ratio.

In summary, the network containing the quasi-compartmental model neuron was able to confirm our hypothesis concerning Plenz and Kitai's (1999) study: that the Ca^{2+} mechanism, described by Beurrier et al. (1999), was the intrinsic property of the STN–GPe circuit which initiated bursting, at a 'native' frequency of ~0.8 Hz, and that cortical input modulated this bursting. To achieve this, we first introduced a modelling approach that phenomenologically replicated each contribution to the membrane potential. Exploration of this neuron model showed that without the Ca^{2+} mechanism bursting could not occur, that noise can assist in the generation of bursting, and that it can act to homogenise unit outputs across a network. With the addition of the quasi-compartmental scheme of spatially separated synapses, we were able to use Plenz and Kitai's data to show that our simplified neuron model (as compared to true multi-compartment models) could successfully account for further aspects of the neurophysiological data.

Some properties of the model neurons introduced in this paper remain to be explored. Two aspects are particularly interesting: first, the extent to which noise causes a homogeneity of unit behaviour in a network needs to be investigated. Preliminary results using an STN–GPe network of simple, non-spiking, leaking integrator model neurons, which contain a version of the Ca^{2+} mechanism, suggest that this 'homogenising' property of noise is specific to spiking model neurons. Furthermore, in the same network, but without axon collaterals within STN, the addition of noise causes burst-firing to cease except at very small magnitude θ_{Ca} in direct contrast to the results reported here. Second, the extent to which synaptic processing (determined by the interplay of addition and shunting inhibition) may be captured by a quasi-compartmental model neuron remains to be established.

Acknowledgements

M. D. Humphries is supported by a studentship from the EPSRC, UK. We would like to thank Peter Redgrave, Tony Prescott and Tom Stafford for many illuminating discussions and for their support. M. D. Humphries would also like to thank Nick Davis for further discussion and suggestions.

References

Atherton, J. F., Gillies, A. J., & Arbuthnott, G. W. (2000). Evidence for the presence of glutamatergic interconnections between neurones in the rat subthalamic nucleus. *European Journal of Neuroscience*, *12* (Supp. 11), 62.20.

Bergman, H., Feingold, A., Nini, A., Raz, A., Slovin, H., Abeles, M., & Vaadia, E. (1998). Physiological aspects of information processing in the basal ganglia of normal and parkinsonian primates. *Trends in Neurosciences*, *21* (1), 32–38.

Bergman, H., Wichmann, T., Karmon, B., & DeLong, M. R. (1994). The primate subthalamic nucleus. II. Neuronal activity in the MPTP model of parkinsonism. *Journal of Neurophysiology*, *72*, 507–520.

Beurrier, C., Bioulac, B., & Hammond, C. (2000). Slowly inactivating sodium current (I_{NaP}) underlies single-spike activity in rat subthalamic neurons. *Journal of Neurophysiology*, *83*, 1951–1957.

Beurrier, C., Congar, P., Bioulac, M., & Hammond, C. (1999). Subthalamic nucleus neurons switch from single spike-activity to burst-firing mode. *Journal of Neuroscience*, *19* (2), 599–609.

Bevan, M. D., & Wilson, C. J. (1999). Mechanisms underlying spontaneous oscillation and rhythmic firing in rat subthalamic neurons. *Journal of Neuroscience*, *19*, 7617–7628.

Bevan, M. D., Clarke, N. P., & Bolam, J. P. (1997). Synaptic integration of functionally diverse pallidal information in the entopeduncular nucleus and subthalamic nucleus in the rat. *Journal of Neuroscience*, *17* (1), 308–324.

Bevan, M. D., Francis, C. M., & Bolam, J. P. (1995). The glutamate-enriched cortical and thalamic input to neurons in the subthalamic nucleus of the rat: convergence with GABA-positive terminals. *Journal of Comparative Neurology*, *361*, 491–511.

Blomfield, S. (1974). Arithmetical operations performed by nerve cells. *Brain Research*, *69*, 115–124.

Borst, A., & Egelhaaf, M. (1994). Dendritic processing of synaptic information by sensory interneurons. *Trends in Neuroscience*, *17*, 257–263.

Brunel, N., & Sergi, S. (1998). Firing frequency of leaky integrate-and-fire neurons with synaptic current dynamics. *Journal of Theoretical Biology*, *195*, 87–95.

Delgado, A., Sierra, A., Querejeta, E., Valdiosera, R. F., & Aceves, J. (2000). Inhibitory control of the GABAergic transmission in the rat neostriatum by D2 dopamine receptors. *Neuroscience*, *95*, 1043–1048.

Fujimoto, K., & Kita, H. (1993). Response characteristics of subthalamic neurons to the stimulation of the sensorimotor cortex in the rat. *Brain Research*, *609*, 185–192.

Gaponov-Grekhov, A. V., & Rabinovich, M. I. (1992). *Non-linearities in action*, Berlin: Springer-Verlag.

Gerfen, C., & Wilson, C. (1996). The basal ganglia. In L. Swanson, A. Bjorklund & T. Hokfelt, *Handbook of chemical neuroanatomy. Vol. 12: integrated systems of the CNS. Part III* (pp. 371–468). Amsterdam: Elsevier.

Gerstner, W. (1999). Spiking neurons. In W. Maass & C. M. Bishop, *Pulsed neural networks* (pp. 3–53). Cambridge, MA: MIT Press.

Gillies, A. J., & Willshaw, D. J. (1998). A massively connected subthalamic nucleus leads to the generation of widespread pulses. *Proceedings of the Royal Society of London-B*, *265*, 2101–2109.

Gillies, A., Atherton, J., Arbuthnott, G., & Willshaw, D. (2000). Glutamatergic interactions between subthalamic nucleus projection neurons. *European Journal of Neurosciences, 12*, (Supp. 11), 226.03.

Gurney, K. (1997). *An introduction to neural networks*, London: UCL Press.

Gurney, K., Prescott, T. J., & Redgrave, P. (2001a). A computational model of action selection in the basal ganglia I: a new functional anatomy. *Biological Cybernetics*, *85*, 401–410.

Gurney, K., Prescott, T. J., & Redgrave, P. (2000b). A computational model of action selection in the basal ganglia II: analysis and simulation of behaviour. *Biological Cybernetics*, *85*, 411–423.

Gurney, K., Redgrave, P., & Prescott, A. (1998). *Analysis and simulation of a model of intrinsic processing in the basal ganglia*. Technical Report AIVRU 131, Dept. Psychology, University of Sheffield.

Hazrati, L. -N., & Parent, A. (1992a). Convergence of subthalamic and striatal afferents at pallidal level in primates: an anterograde-labeling study with biocytin and PHA-L. *Brain Research*, *569*, 336–340.

Hazrati, L. -N., & Parent, A. (1992b). Differential patterns of arborisation of striatal and subthalamic fibers in the two pallidal segments in primates. *Brain Research*, *598*, 311–315.

Hikosaka, O. (1991). Basal ganglia—possible role in motor coordination and learning. *Current Opinion in Neurobiology*, *1*, 638–643.

Hoover, J. E., & Strick, P. L. (1993). Multiple output channels in the basal ganglia. *Science*, *259*, 819–821.

Hoover, J. E., & Strick, P. L. (1999). The organization of cerebellar and basal ganglia outputs to primary motor cortex as revealed by retrograde transneuronal transport of herpes simplex virus type 1. *Journal of Neuroscience*, *19* (4), 1446–1463.

Hsu, K.-S., Huang, C.-C., Yang, C.-H., & Gean, P.-W. (1995). Presynaptic D2 dopaminergic receptors mediate inhibition of excitatory synaptic transmission in the rat neostriatum. *Brain Research*, *690*, 264–268.

Humphries, M. D., & Gurney, K. (1999). *A computational model of action selection in the basal ganglia: thalamic and cortical interactions*. Technical Report AIVRU 132, Dept. Psychology, University of Sheffield.

Joel, D., & Weiner, L. (1997). The connections of the primate subthalamic nucleus: indirect pathways and the open-interconnected scheme of basal gangliathalamocortical circuitry. *Brain Research Reviews*, *23*, 62–78.

Kim, U., & McCormick, D. A. (1998). The functional influence of burst and tonic firing mode on synaptic interactions in the thalamus. *Journal of Neuroscience*, *18* (22), 9500–9516.

Kim, U., Sanchez-Vives, M. V., & McCormick, D. A. (1997). Functional dynamics of the GABAergic inhibition in the thalamus. *Science*, *278*, 130–134.

Maass, W. (1997). Networks of spiking neurons: the third generation of neural network models. *Neural Networks*, *10*, 1659–1671.

Magill, P. J., Bolam, J. P., & Bevan, M. D. (2000). Relationship of activity in the subthalamic nucleus–globus pallidus network to cortical electroencephalogram. *Journal of Neuroscience*, *20*, 820–833.

Magnin, M., Morel, A., & Jeanmonod, D. (2000). Single-unit analysis of the pallidum, thalamus and subthalamic nucleus in parkinsonian patients. *Neuroscience*, *96*, 549–564.

Plenz, D., & Kitai, S. (1999). A basal ganglia pacemaker formed by the subthalamic nucleus and external globus pallidus. *Nature*, *400*, 677–682.

Raz, A., Vaadia, E., & Bergman, H. (2000). Firing patterns and correlations of spontaneous discharge of pallidal neurons in the normal and the tremulous 1-methyl-4-phenyl-1,2,3,6-tetrahydropyridine vervet model of parkinsonism. *Journal of Neuroscience*, *20*, 8559–8571.

Redgrave, P., Prescott, T. J., & Gurney, K. (1999). The basal ganglia: a vertebrate solution to the selection problem? *Neuroscience*, *89* (4), 1009–1023.

Ross, S. M. (1985). *Introduction to probability models*, (3rd ed). Orlando: Academic Press.

Rowat, P. F., & Selverston, A. I. (1997). Synchronous bursting can arise from mutual excitation, even when individual cells are not endogenous bursters. *Journal of Computational Neuroscience*, *4*, 129–139.

Segev, I., Fleshman, J. W., & Burke, R. E. (1989). Compartmental models of complex neurons. In C. Koch & I. Segev, *Methods in neuronal modeling* (pp. 63–96). Cambridge, MA: MIT Press.

Segundo, J. P., Stiber, M., & Vibert, J. -F. (1995). Synaptic coding of spike trains. In M. A. Arbib, *The handbook of brain theory and neural networks* (pp. 953–956). Cambridge, MA: MIT Press.

Shepherd, G. M., & Brayton, R. K. (1987). Logic operations are properties of computer-simulated interaction between excitable dendritic spines. *Neuroscience*, *21*, 151–165.

Turner, R. S., & DeLong, M. R. (2000). Corticostriatal activity in primary motor cortex of the macaque. *Journal of Neuroscience*, *20*, 7096–7108.

Ulrich, D., & Huguenard, J. R. (1997). GABAa-receptor-mediated rebound burst firing and burst shunting in the thalamus. *Journal of Neurophysiology*, *78*, 1748–1751.

White, G., Lovinger, D. M., & Weight, F. F. (1989). Transient low-threshold Ca^{2+} current triggers burst firing through an after-depolarizing potential in an adult mammalian neuron. *Proceedings of the National Academy of Sciences USA*, *86*, 6802–6806.

Wichmann, H., Bergman, H., & DeLong, M. (1994). The primate subthalamic nucleus. I. Functional properties in intact animals. *Journal of Neurophysiology*, *72*, 494–506.

Wickens, B. G., & Wilson, C. J. (1998). Regulation of action-potential firing in spiny neurons of the rat neostriatum in vivo. *Journal of Neurophysiology*, *79*, 2358–2364.